

RESEARCH ARTICLE | OCTOBER 12 2021

Spin-lattice angular momentum transfer of localized and valence electrons in the demagnetization transient state of gadolinium ^F

Special Collection: [Ultrafast and Terahertz Spintronics](#)

Régis Decker ; Artur Born; Kari Ruotsalainen; Karl Bauer ; Robert Haverkamp; Robby Büchner; Annette Pietzsch ; Alexander Föhlisch

Check for updates

Appl. Phys. Lett. 119, 152403 (2021)
<https://doi.org/10.1063/5.0063404>

View Online

Export Citation

CrossMark

Articles You May Be Interested In

Resonant inelastic scattering at the 3d and 4d resonances of LaAlO₃

AIP Conference Proceedings (February 2000)

Physical Interpretation of Glory Undulations in Scattering Cross Sections

J. Chem. Phys. (September 2003)



Cut Hall measurement time in *half* using an M91 FastHall™ controller



Also available as part of a tabletop system and an option for your PPMS® system

Spin-lattice angular momentum transfer of localized and valence electrons in the demagnetization transient state of gadolinium

Cite as: Appl. Phys. Lett. **119**, 152403 (2021); doi: [10.1063/5.0063404](https://doi.org/10.1063/5.0063404)

Submitted: 14 July 2021 · Accepted: 20 September 2021 ·

Published Online: 12 October 2021



View Online



Export Citation



CrossMark

Régis Decker,^{1,a)}  Artur Born,^{1,2} Kari Ruotsalainen,¹ Karl Bauer,¹  Robert Haverkamp,^{1,2} Robby Büchner,^{1,2} Annette Pietzsch,¹  and Alexander Föhlisch^{1,2,a)} 

AFFILIATIONS

¹Institute for Methods and Instrumentation for Synchrotron Radiation Research PS-ISRR, Helmholtz-Zentrum Berlin für Materialien und Energie, Albert-Einstein-Strasse 15, 12489 Berlin, Germany

²Institut für Physik und Astronomie, Universität Potsdam, Karl-Liebknecht-Strasse 24-25, 14476 Potsdam, Germany

Note: This paper is part of the APL Special Collection on Ultrafast and Terahertz Spintronics.

^{a)}Authors to whom the correspondence should be addressed: regis.decker@helmholtz-berlin.de and alexander.foehlich@helmholtz-berlin.de

ABSTRACT

The electron–phonon scattering is one of the main microscopic mechanisms responsible for the spin-flip in the transient state of ultrafast demagnetization. Here, we present an experimental determination of the temperature-dependent electron–phonon scattering rate in Gd. Using a static x-ray emission spectroscopy method, where the reduction of the decay peak intensities when increasing the temperature is quantified, we measure independently the electron–phonon scattering rate for the 5*d* and the 4*f* electrons. We deduce the temperature dependence of scattering for the 5*d* electrons, while no effect on the phonon population is observed for the 4*f* electrons. Our results suggest that the ultrafast magnetization dynamics in Gd is triggered by the spin-flip in the 5*d* electrons. We also evidence the existence of a temperature threshold, above which spin-flip scattering of the 5*d* electrons takes place. We deduce that during the transient state of ultrafast demagnetization, the exchange energy between 5*d* electrons has to be overcome before the microscopic electron–phonon scattering process can occur.

© 2021 Author(s). All article content, except where otherwise noted, is licensed under a Creative Commons Attribution (CC BY) license (<http://creativecommons.org/licenses/by/4.0/>). <https://doi.org/10.1063/5.0063404>

The microscopic mechanisms of spin relaxation in magnets placed out of equilibrium by ultrashort laser pulses are still under debate. The empirical three-temperature model (3TM) describes such nonequilibrium states in 3*d* magnets as three interacting distinct reservoirs: the electrons (el), the lattice (ph), and the spins (sp), which exchange energy (heat) only.¹ While the 3TM can predict the sub-ps ultrafast evolution of subsystems in 3*d* magnets and, in particular, the sub-ps demagnetization time, it does not consider the angular momentum conservation of the system and its transfer between subsystems. Later, Koopmans *et al.* introduced the so-called microscopic 3TM (M3TM), which explicitly takes the conservation of angular momentum into account.² In the M3TM, the energy transfer from the hot electron reservoir provides the energy for demagnetization, and the angular momentum transfer is driven by an Elliott-Yafet-like mechanism (EY), where spin-flip events are accompanied by the creation or suppression of phonons during el-ph scattering.^{3,4}

In rare earth magnets, the total magnetic moment is shared by the itinerant 5*d*(6*sp*) and by the localized 4*f* electrons. Early investigations of ultrafast demagnetization of Gd by Vaterlaus *et al.* measured a timescale of 100 ± 80 ps,⁵ i.e., two to three orders of magnitude slower than for 3*d* magnets.^{2,6–13} Such disparate time scales are a clear indication of an incomplete microscopic description of ultrafast demagnetization. This legitimated the idea of differentiating the electron and spin reservoirs themselves into two components, the 4*f* localized states and the itinerant 5*d* band, coupled by the strong intra-atomic exchange interaction $J_{intra} = 130$ meV. Here again, the M3TM model clarifies the discrepancy, by proposing that the ratio of the Curie temperature and the atomic magnetic moment T_C/μ_{at} is the key parameter underlying the different timescales.

More recently, however, B. Frietsch *et al.* measured a different demagnetization time between the 5*d* (0.8 ps) and the 4*f* (14 ps) spins.¹⁴ In an extended 3TM model (E3TM), built on the

Landau–Lifschitz–Gilbert (LLG) model, the experimental observations were interpreted by assuming that the $5d$ spins couple to the hot electron bath and the $4f$ to the phonon bath, the latter being thermalized later in the nonequilibrium state.^{14,15} Nevertheless, the E3TM does not consider the conservation of angular momentum in the system. Moreover, in regard to the high intra-atomic exchange, such a disparate timescale between the $5d$ and $4f$ demagnetization is *a priori* in contradiction with the M3TM. So far, no experimental work has evidenced a distinct angular momentum transfer process for the $4f$ and the $5d$ spins.

In this article, we present the temperature-dependent el-ph scattering rate of the localized $4f$ and of the itinerant $5d$ electrons of Gd independently. The rates are deduced from the evolution of features in x-ray emission spectroscopy (XES) with the temperature. Our experimental method is built on the core-hole clock method, where the core-hole lifetime is used as reference to determine timescales of events such as scattering that occur in the intermediate state of the XES process.^{16–22} We show, on the one hand, the absence of temperature dependence of features linked to the decay of $4f$ electrons and, on the other hand, a reduction of the emission peak intensity corresponding to the decay of the $5d$ electrons. We interpret these observations in terms of an absence of el-ph scattering for the $4f$ electrons and an enhancement of the el-ph scattering rate with the temperature for the $5d$ electrons. Our measurements also suggest the existence of a threshold temperature for the el-ph scattering of $5d$ electrons. We link this threshold to the $5d$ exchange energy, which has to be overcome to trigger the el-ph scattering and below which no spin-flip occurs.

Our experiments were performed with the SolidFlexRIXS endstation on the U49–2_PGM-1, the UE112_PGM-1, and the UE52_SGM beamlines at BESSY II during the multi-bunch operation mode. The sample was heated by electron bombardment from a hot filament placed behind the sample. Prior to data acquisition, the Gd sample was cleaned by annealing up to 775 K for segregation and degassing of bulk impurities. The system thermalized a few minutes before each data acquisition. The base pressure was in the low 10^{-8} mbar range but rose up to the 10^{-7} mbar range for the highest temperatures. The temperature-dependent data acquisitions for the $4f$ (Gd N_5 excitation) and the $5d$ (Gd $N_{2,3}$ excitation) were performed independently.

In order to observe the temperature dependence of spectral features corresponding to the radiative decay from the localized $4f$ states, we used excitation energies in the region of the Gd N_5 edge (excitation of the $4d$ core state). Figure 1(a) is a resonant inelastic x-ray scattering (RIXS) map ($\hbar\omega_{em}$ vs $\hbar\omega_{exc}$) in this energy region acquired at room temperature. We distinguish three main features. The highest emission energy feature corresponds to the elastic peak ($\hbar\omega_{em} = \hbar\omega_{exc}$). The lowest energy feature (visible at $\hbar\omega_{em} < 125$ eV) is a doublet feature characterized by a broad line at a constant energy difference of $\hbar\Delta\omega = \hbar\omega_{em} - \hbar\omega_{exc} = 28$ eV with respect to the elastic line and a second broad line at a constant energy difference of $\hbar\Delta\omega = 34$ eV. This constant $\hbar\Delta\omega$ is indicative of a resonant x-ray Raman process.²³ This doublet feature corresponds to the decay from the $4d^9 5p^6 4f^8$ intermediate state to the $4d^{10} 5p^5 4f^8$ final state, and the two lines correspond to the decay from the spin-orbit-split $5p_{1/2}$ and $5p_{3/2}$ states.

The third main feature is characterized by three narrow lines at $\hbar\Delta\omega = 4, 5,$ and 6 , respectively, and visible for $E_{exc} = 143$ – 145 eV. At this energy, the system is resonantly excited from the $^8S_{7/2}$

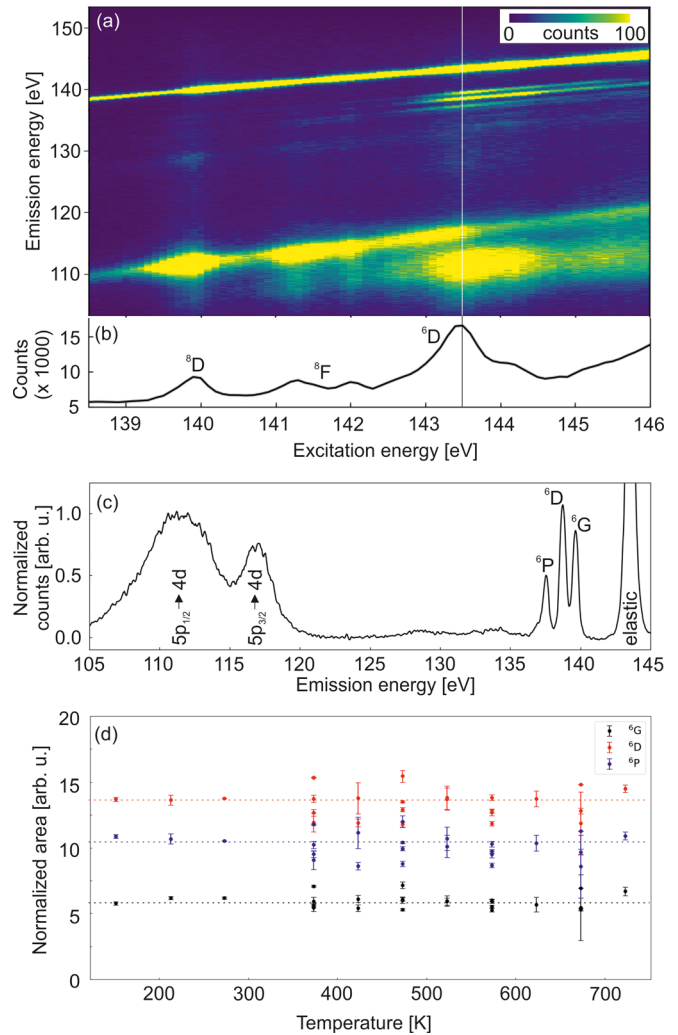


FIG. 1. Temperature dependence of the $4f$ decay features. (a) RIXS-map in the Gd N_5 edge energy region acquired at room temperature. The white line at $E_{exc} = 143.5$ eV corresponds to the spectrum shown in (c). (b) Absorption spectroscopy in the energy region corresponding to the RIXS map, measured in the total electron yield mode. (c) RIXS spectrum acquired at $E_{exc} = 143.5$ eV, normalized against the $5p_{1/2} \rightarrow 4d$ decay peak (see the text). (d) Areas of the 6P , 6D , and 6G multiplet peaks as a function of the temperature. Colored dotted lines are guides to the eyes.

($4d^{10} 5p^6 4f^7$) ground state to the 6D ($4d^9 5p^6 4f^8$) intermediate state. The two other absorption pre-peaks correspond to the $^8S_{7/2}$ to 8D and 8F transitions, as labeled in Fig. 1(b). The three lines feature in the RIXS-map correspond to transitions from the 6D intermediate state to the 6G , 6D and 6P ($4d^{10} 5p^6 4f^7$) final state multiplet.^{24,25} Thus, this feature corresponds to the decay from the $4f$ state to the $4d$ core-hole and is accordingly the feature of interest to observe a possible scattering effect of $4f$ localized electrons.

A typical emission spectrum acquired in the case of a $^8S_{7/2} \rightarrow ^6D$ excitation at $E_{exc} = 143.5$ eV and normalized against the $5p_{1/2} \rightarrow 4d$ emission peak is shown in Fig. 1(c). The $5p_{1/2,3/2} \rightarrow 4d$ decay features

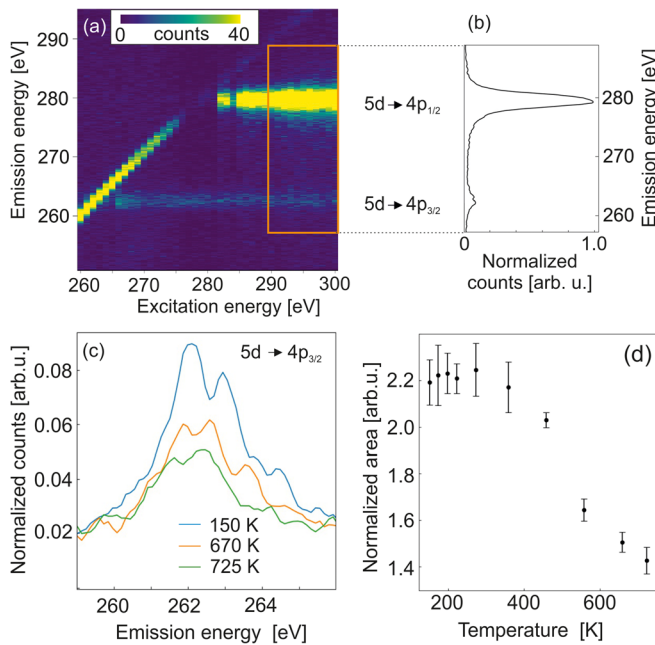


FIG. 2. Temperature-dependence of the $5d$ decay spectral features. (a) RIXS-map in the Gd $N_{2,3}$ edge energy region acquired at $T = 150$ K. (b) Sum of spectra in the energy region $E_{exc} = 290$ to 300 eV (corresponding to the orange rectangle in (a)), normalized against the $5d \rightarrow 4p_{1/2}$ peak. (c) Zoom in the $5d \rightarrow 4p_{3/2}$ peak for $T = 150, 670,$ and 725 K. (d) Normalized $5d \rightarrow 4p_{3/2}$ peak area vs the temperature.

are independent of any process occurring in the $4f$ state. In addition, since the $5p$ shell is fully occupied in the $4d^9 5p^6 4f^{86} D$ intermediate state, $5p$ electrons cannot scatter. Therefore, we assume that the intensity of the corresponding emission peak does not change when changing the temperature, which allows the use of the $5p_{1/2} \rightarrow 4d$ feature as a reference for the normalization of emission spectra.^{16,26}

We monitored the evolution of the area of each emission peak of the final state multiplet as a function of the temperature. As shown in Fig. 1(d), no dependence of the peak areas on the temperature is observed within the studied temperature range (150–750 K). This indicates the absence of temperature-dependent electron scattering for the $4f$ shell.

To assess the decay of $5d$ electrons, we tuned the incident photon energy to the Gd $N_{2,3}$ edge energy region $E_{exc} = 260$ – 300 eV. Figure 2(a) shows a measured RIXS map in this energy region. The diagonal line visible mostly at $E_{exc} = 260$ – 275 eV corresponds the elastic peak (zero loss). The two horizontal lines in the map correspond to the $5d \rightarrow 4p_{1/2}$ and $5d \rightarrow 4p_{3/2}$ decays, as indicated in Fig. 2(b). The spectra in Fig. 2(b) represent the sum of spectra in the $E_{exc} = 290$ – 300 eV energy region, normalized against the integrated $5d \rightarrow 4p_{1/2}$ peak intensity. The reason for this normalization is discussed below. Strictly, it implies that we set a constant $5d \rightarrow 4p_{1/2}$ peak intensity and that only the ratio of the $5d \rightarrow 4p_{1/2}$ and $5d \rightarrow 4p_{3/2}$ peaks can be considered in the following. Figure 2(c) shows a zoom in the $5d \rightarrow 4p_{3/2}$ for the three representative temperatures $T = 150, 670,$ and 725 K, where a clear decrease in intensity is visible. The evolution of the $5d \rightarrow 4p_{3/2}$ peak area with the temperature in the investigated temperature range from 150 to 725 K is shown in

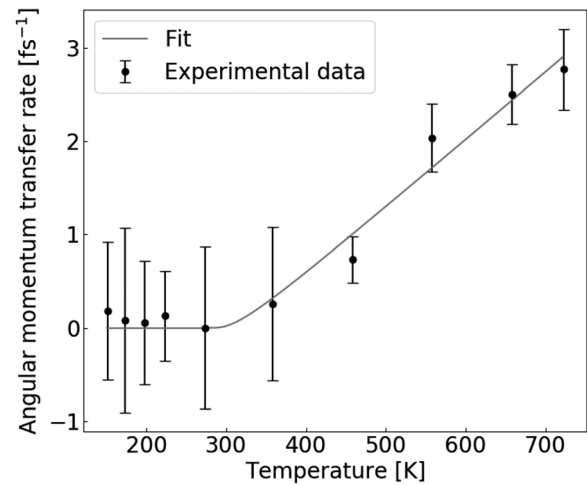


FIG. 3. Angular momentum transfer rate vs temperature. Data points (black dots) are derived from the experimental data shown in Fig. 3(d). The fit includes two temperature regions. Above 270 K, data points are fitted by the Bose–Einstein distribution. Below 270 K, data points are fitted by an horizontal line at zero rate.

Fig. 2(c). A constant peak area for $T < 270$ K is followed by a steep decrease up to 725 K. It is interesting to note that the decrease starts at a temperature close to the Curie temperature of Gd (292 K).

We present in the following our interpretation for the observed reduction of the $5d \rightarrow 4p_{3/2} / 4p_{1/2}$ emission peak with the temperature and its absence for the $4f \rightarrow 4d$ multiplet features. The interpretation is built on the basic fact that a modification of the emission peak intensity reflects a change in the density of electrons available for decay.

Scattering induces a linear or an angular momentum transfer, which decreases the electron density available for radiative decay. Earlier work on Si has shown that the distinction between linear and angular momentum can be made by considering resonant and continuum excitation.¹⁷ However, for the Gd $4f$ decay, the linear momentum transfer can be ruled out as the origin of the spectral modifications due to the dispersionless nature of the localized state. For the Gd $5d$ decay, we consider detuned excitations only, i.e., away from resonance, for the spectral temperature dependence shown in Figs. 2(c) and 2(d). In this situation, the linear momentum transfer would also not affect the spectra since all k indistinctly participate to the core-hole decay. Thus, we interpret possible spectral changes as a consequence of scattering-driven angular momentum transfer for both the $4f$ and the $5d$ decays. According to the dipole selections rules, the electrons that undergo an angular momentum change during the core-hole lifetime do not participate in the decay. This leads to a reduction of the decay probability, visible as a reduction of the corresponding emission peak intensity.

Therefore, the constant peak area of the $4f$ decay features shown in Fig. 1(d) reflects the absence of el-ph scattering-driven angular momentum transfer for the $4f$ electrons in the intermediate state. This result is a clear indication that the microscopic process of ultrafast demagnetization is not governed by the $4f$ el-ph angular momentum transfer.

In contrast, a loss of intensity is visible for the $5d \rightarrow 4p_{3/2}$ peak in Figs. 2(c) and 2(d), when spectra are normalized against the

$5d \rightarrow 4p_{1/2}$ peak. Note that within the framework of this interpretation, scattering can only decrease the density of electrons available for the core-hole decay and, thus, the emission peak intensities. This is the reason why spectra in Figs. 2(b) and 2(c) were normalized against the $5d \rightarrow 4p_{1/2}$ peak intensity. This normalization assumes no temperature dependence of the $5d \rightarrow 4p_{1/2}$ peak intensity and, thus, gives a lower limit of the scattering rate. Similar to the previous work on Ni, Cu, and FeNi, we consider no orbital angular momentum transfer, i.e., d to s or d to p because of the low s and p density of states, and we attribute the angular momentum transfer of $5d$ electrons directly to the el-ph spin-flip.^{16,26} Therefore, our results evidence an EY scenario driven solely by the $5d$ electrons for the ultrafast demagnetization of Gd.

From the evolution of the $5d \rightarrow 4p_{3/2}$ peak intensity vs temperature shown in Fig. 2(d), we deduce the el-ph scattering driven spin-flip rate $R(T)$, following the well-established procedure developed by us for the pure Ni and FeNi alloys.^{16,26}

The experimental points from Fig. 2(d) are used to derive the spin-flip rate $R(T)$ using the core-hole clock method^{18–22}

$$R(T) = \frac{1}{\tau_{\text{core-hole}}} \cdot \frac{A_{\text{inc}}(T)}{A_{\text{coh}}} = \frac{1}{\tau_{\text{core-hole}}} \cdot \frac{A_{\text{cold}} - A_{\text{hot}}(T)}{A_{\text{cold}}}, \quad (1)$$

where $\tau_{\text{core-hole}} = 0.13$ fs is the $4p_{3/2}$ core-hole lifetime deduced from the atomic level width.²⁷ Note that this core-hole lifetime is an order of magnitude shorter than those of Fe and Ni.²⁶ Here, A_{cold} is the peak area at 270 K, which shows the highest area in Fig. 2(d). $A_{\text{inc}}(T) = A_{\text{cold}} - A_{\text{hot}}(T)$, the incoherent part of the peak, which is the part lost due to the scattering and $A_{\text{coh}} = A_{\text{cold}}$ is the part not affected by it.

The evolution of $R(T)$ clearly shows a constant zero rate below 270 K, defined as the threshold temperature T_0 in the following, and an almost linear increase above threshold. In order to fit the experimental points, we considered these two temperature regions independently. Below T_0 , data points are fitted by an horizontal line at zero rate. Above T_0 , we fit the experimental data by the sum of a constant rate C_{indep} independent of the temperature and of a temperature-dependent part proportional to the Bose–Einstein distribution

$$R(T) = C_{\text{indep}} + C_{\text{dep}} \cdot \frac{1}{e^{k_b(T-T_0)} - 1}. \quad (2)$$

Here, we used the phonon energy mean value $E_{ph} = 9.64$ meV derived from the phonon distribution vs energy from Ref. 28.

This different behavior below and above a threshold temperature is comparable to previous observations for FeNi alloys.²⁶ In that case, it was also established that a temperature threshold has to be overcome in order to trigger the el-ph driven spin-flip scattering, and this threshold is linked to the magnitude of the intra-sublattice exchange energies.²⁹ For pure Ni, this threshold is not observed due to the relatively low exchange energy, below 1 meV.^{16,26} In Gd, the exchange energy in the $5d$ band is 5.9 meV. This value is lower than the one of iron in iron–nickel alloys, which is on the order of 10–20 meV, depending on the stoichiometry and for which a threshold temperature of 800 K is deduced. Thus, the lower threshold temperature of Gd in comparison to FeNi systems is consistent with a lower exchange energy to be overcome before the el-ph scattering driven spin-flip initiates.

The threshold temperature corresponds to the T_C of Gd. One notes that we observed such a threshold at T_C for the Fe sublattices in

FeNi alloys. However, no threshold was observed for the Ni sublattices in the same alloys (and, thus, with the same T_C)²⁶ nor for pure Ni,¹⁶ the latter probably because of the relatively low T_C of Ni.

One notes that in the Bose–Einstein distribution fit function, the temperature is lowered by this threshold temperature T_0 . Physically, this means that no phonons are available for the scattering below T_0 and that the phonons start to scatter only at and above the threshold temperature. This aspect was not visible in the previous work with Ni and FeNi alloys due to the much lower scattering rate in these systems.²⁶

Dynamic physical systems such as magnets placed in a transient out-of-equilibrium state after an ultrashort laser pulse evolve with time and are characterized by time-dependent transfer of energy and angular momentum between the different subsystems. Our static experiments, where the entire system is placed in equilibrium and at a fixed temperature, overcome this time dependence. In particular, this allows us to identify the existence of the two different regimes, associated with different microscopic processes, which occur at different times after the laser pulse in the framework of ultrafast magnetism.

Our study highlights different aspects of the microscopic mechanisms at play during the transient demagnetization state of Gd. First, it evidences the absence of el-ph scattering driven spin-flip of the $4f$ electrons. On the contrary, a clear temperature dependence of the spin-flip rate is observed for $5d$ electrons. We interpret this dependence in terms of an EY scattering spin-flip microscopic mechanism for the $5d$ electrons. Second, our observations indicate that the threshold behavior of the spin-flip scattering is defined by the $5d$ exchange energy, similarly to what is observed for FeNi alloys.²⁶ This point further evidences the interplay of different processes in the non-equilibrium state of ultrafast magnetism. Finally, our results show that the ultrafast demagnetization is driven by the EY scattering in the $5d$ band,² whereas el-ph scattering driven spin-flip involving $4f$ electrons could not be detected. Our state specific scattering rates are fully in line with the recently reported 17.5 times slower demagnetization dynamic of $4f$ (14 ps) vs $5d$ (0.8 ps) electrons in Gd.¹⁴ However, the absence of the temperature-dependent el-ph scattering rate for the localized $4f$ electrons indicates an additional spin-flip mechanism beyond direct EY scattering that unambiguously governs the $5d$ electrons.

See the [supplementary material](#) for further details on the methodology and experiments.

DATA AVAILABILITY

The data that support the findings of this study are available from the corresponding authors upon reasonable request.

REFERENCES

- ¹E. Beaurepaire, J.-C. Merle, A. Daunois, and J.-Y. Bigot, *Phys. Rev. Lett.* **76**, 4250 (1996).
- ²B. Koopmans, G. Malinowski, F. Dalla Longa, D. Steiauf, M. Fähnle, T. Roth, M. Cinchetti, and M. Aeschlimann, *Nat. Mater.* **9**, 259 (2010).
- ³R. J. Elliott, *Phys. Rev.* **96**, 266 (1954).
- ⁴Y. Yafet, *Solid State Physics*, edited by F. Seitz and D. Turnbull (Academic, 1963), Vol. 14.
- ⁵A. Vaterlaus, T. Beutler, D. Guarisco, M. Lutz, and F. Meier, *Phys. Rev. B* **46**, 5280 (1992).
- ⁶M. Krauß, T. Roth, S. Alebrand, D. Steil, M. Cinchetti, M. Aeschlimann, and H. C. Schneider, *Phys. Rev. B* **80**, 180407 (2009).

- ⁷C. Stamm, T. Kachel, N. Pontius, R. Mitzner, T. Quast, K. Hollmack, S. Khan, C. Lupulescu, E. F. Aziz, M. Wietstruk *et al.*, *Nat. Mater.* **6**, 740 (2007).
- ⁸J. Hohlfield, E. Matthias, R. Knorren, and K. H. Bennemann, *Phys. Rev. Lett.* **78**, 4861 (1997).
- ⁹H.-S. Rhie, H. A. Dürr, and W. Eberhardt, *Phys. Rev. Lett.* **90**, 247201 (2003).
- ¹⁰K. C. Kuiper, T. Roth, A. J. Schellekens, O. Schmitt, B. Koopmans, M. Cinchetti, and M. Aeschlimann, *Appl. Phys. Lett.* **105**, 202402 (2014).
- ¹¹M. Cinchetti, M. Sánchez Albaneda, D. Hoffmann, T. Roth, J.-P. Wüstenberg, M. Krauß, O. Andreyev, H. C. Schneider, M. Bauer, and M. Aeschlimann, *Phys. Rev. Lett.* **97**, 177201 (2006).
- ¹²A. Weber, F. Pressacco, S. Günther, E. Mancini, P. M. Oppeneer, and C. H. Back, *Phys. Rev. B* **84**, 132412 (2011).
- ¹³E. Carpena, E. Mancini, C. Dallera, M. Brenna, E. Puppini, and S. D. Silvestri, *Phys. Rev. B* **78**, 174422 (2008).
- ¹⁴B. Frietsch, J. Bowlan, R. Carley, M. Teichmann, S. Wienholdt, D. Hinzke, U. Nowak, K. Carva, P. M. Oppeneer, and M. Weinelt, *Nat. Commun.* **6**, 8262 (2015).
- ¹⁵S. Wienholdt, D. Hinzke, K. Carva, P. M. Oppeneer, and U. Nowak, *Phys. Rev. B* **88**, 020406 (2013).
- ¹⁶R. Decker, A. Born, R. Büchner, K. Ruotsalainen, C. Strählmann, S. Neppel, R. Haverkamp, A. Pietzsch, and A. Föhlisch, *Sci. Rep.* **9**, 8977 (2019).
- ¹⁷M. Beye, F. Hennies, M. Deppe, E. Suljoti, M. Nagasono, W. Wurth, and A. Föhlisch, *Phys. Rev. Lett.* **103**, 237401 (2009).
- ¹⁸A. Föhlisch, P. Feulner, F. Hennies, A. Fink, D. Menzel, D. Sanchez-Portal, P. M. Echenique, and W. Wurth, *Nature* **436**, 373 (2005).
- ¹⁹O. Björneholm, A. Nilsson, A. Sandell, B. Hernnäs, and N. Mårtensson, *Phys. Rev. Lett.* **68**, 1892 (1992).
- ²⁰W. Wurth and D. Menzel, *Chem. Phys.* **251**, 141 (2000).
- ²¹P. A. Brühwiler, O. Karis, and N. Mårtensson, *Rev. Mod. Phys.* **74**, 703 (2002).
- ²²A. Föhlisch, D. Menzel, P. Feulner, M. Ecker, R. Weimar, K. Kostov, G. Tyuliev, S. Lizzit, R. Larciprete, F. Hennies *et al.*, *Chem. Phys.* **289**, 107 (2003).
- ²³J. J. Gallet, J. M. Mariot, C. F. Hague, F. Sirotti, M. Nakazawa, H. Ogasawara, and A. Kotani, *Phys. Rev. B* **54**, R14238 (1996).
- ²⁴A. Moewes, T. Eskildsen, D. L. Ederer, J. Wang, J. McGuire, and T. A. Callcott, *Phys. Rev. B* **57**, R8059 (1998).
- ²⁵Y.-C. Shao, L. A. Wray, S.-W. Huang, Y.-S. Liu, W. Song, S. Yang, Y.-D. Chuang, J. Guo, and W.-F. Pong, *Sci. Rep.* **7**, 8125 (2017).
- ²⁶A. Born, R. Decker, R. Büchner, R. Haverkamp, K. Ruotsalainen, K. Bauer, A. Pietzsch, and A. Föhlisch, *Sci. Rep.* **11**, 1883 (2021).
- ²⁷J. Campbell and T. Papp, *At. Data Nucl. Data Tables* **77**, 1 (2001).
- ²⁸R. R. Rao and C. Menon, *J. Phys. Chem. Solids* **35**, 425 (1974).
- ²⁹J. H. Mentink, J. Hellsvik, D. V. Afanasiev, B. A. Ivanov, A. Kirilyuk, A. V. Kimel, O. Eriksson, M. I. Katsnelson, and T. Rasing, *Phys. Rev. Lett.* **108**, 057202 (2012).